Stress-Strain Behavior of Thermoplastic Polyurethane

H.J. Qi[1,2], M.C. Boyce[1,*]

[1]Department of Mechanical Engineering

Massachusetts Institute of Technology

Cambridge, MA 02139

[2]Department of Mechanical Engineering

University of Colorado

Boulder, CO 80309

Submitted in December 2003

Revised in July 2004

Submitted to Mechanics of Materials

[*] Corresponding author. Tel: 1-617-253-2342; fax: 1-617-258-8742

E-mail address: mcboyce@mit.edu

Stress-Strain Behavior of Thermoplastic Polyurethane

H.J. Qi[1,2], M.C. Boyce[1]

[1]Department of Mechanical Engineering, Massachusetts Institute of Technology
Cambridge, MA 02139

[2]Department of Mechanical Engineering, University of Colorado
Boulder, CO 80309

Submitted in December 2003

Revised in July 2004

Abstract

The large strain nonlinear stress-strain behavior of thermoplastic polyurethanes (TPUs) exhibits strong hysteresis, rate dependence and softening. Thermoplastic polyurethanes are copolymers composed of hard and soft segments. The hard and soft segments phase separate to form a microstructure of hard and soft domains typically on a length scale of a few tens of nanometers. Studies have revealed this domain structure to evolve with deformation; this evolution is thought to be the primary source of hysteresis and cyclic softening. In this paper, experiments and a constitutive model capturing the major features of the stress-strain behavior of TPUs, including nonlinear hyperelastic behavior, time dependence, hysteresis, and softening, are presented. The model is based

on the morphological observations of TPUs during deformation. A systematic method to estimate the material parameters for the model is presented. Excellent agreement between experimental results and model predictions of various uniaxial compression tests confirms the efficacy of the proposed constitutive model.

Keyword: Softening; Mullins' Effect; Stress-Strain Behavior; Thermoplastic Polyurethane Elastomer; Rubber.

1. Introduction

The first commercial thermoplastic polyurethanes (TPUs) were established in Germany by Bayer-Fabenfabriken and in the U.S. by B.F. Goodrich in the 1950s (Schollenbenger et al., 1958). The Alliance for the Polyurethane Industry (API) describes TPUs as "bridging the gap between rubber and plastics", since TPUs offer the mechanical performance characteristics of rubber but can be processed as thermoplastics. This special niche of TPUs among other polymers and elastomers imparts high elasticity combined with high abrasion resistance, and results in a wide array of applications ranging from ski boots and footwear to gaskets, hoses, and seals.

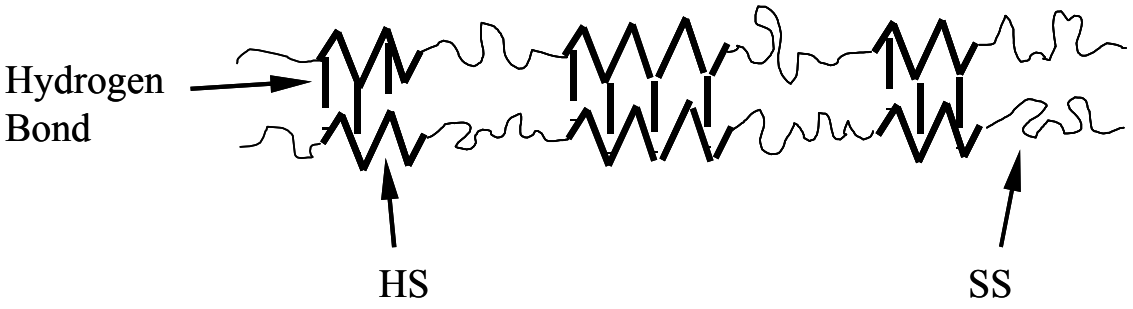

Figure 1: The alternating structure of TPUs. HS: Hard segment; SS: Soft Segment.

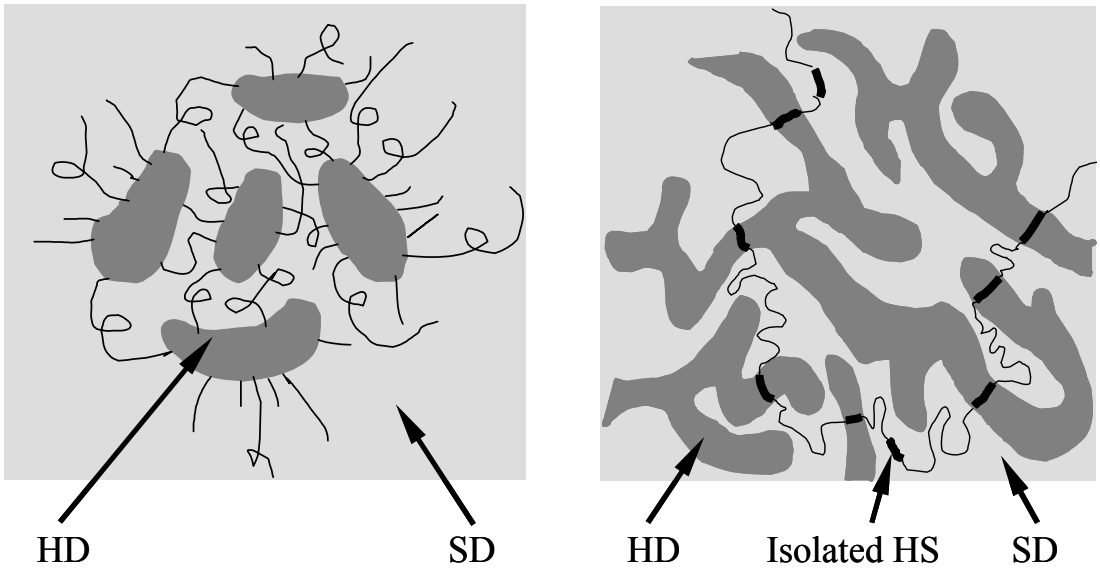

(a) (b)

Figure2: Hard domains (HD) and soft domains (SD) of TPUs with (a) a low hard segment content (adopted from Petrovic and Ferguson, 1991); (b) a high hard segment content (adopted from Estes et al. (1971) and Petrovic and Ferguson (1991)). Isolated hard segments (HS) seen in (b).

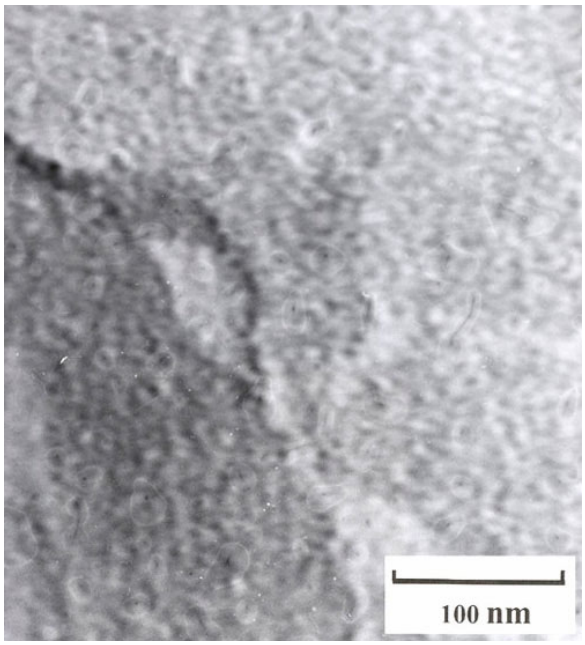

Figure 3: Transmission Electron Microscope (TEM) image of osmium tetroxide tainted TPU (57% soft segment and 43% hard segment). The light regions are hard domains and the dark regions are soft domains.

Thermoplastic polyurethanes are randomly segmented copolymers (Hepburn, 1982) composed of hard and soft segments forming a two-phase microstructure (Figure 1). Generally, phase separation occurs in most TPUs due to the intrinsic incompatibility between the hard segments and soft segments: the hard segments, composed of polar materials, can form carbonyl to amino hydrogen bonds and thus tend to cluster or aggregate into ordered hard domains, whereas the soft segments form amorphous domains. Phase separation, however, is often incomplete, i.e., some of the hard segments are isolated in the soft domains as illustrated schematically in Figure 2(b) (Petrovic and Ferguson, 1991). In many TPUs, the hard domains are immersed in a rubbery soft segment matrix (Wang and Cooper, 1983; Petrovic and Ferguson, 1991). Depending on the hard segment content, the morphology of the hard domains changes from one of isolated domains (Figure 2(a), (Petrovic and Ferguson, 1991)) to one of interconnected domains (Figure 2(b))(Estes et al., 1971; Petrovic and Ferguson, 1991). Using TEM (Transmission Electron Microscope), the interconnected domain structure was verified for the TPU[1] used in this research as shown in Figure 3. The domain size in Figure 3 is 10~20nm, which is consistent with observations on various other TPUs (e.g., Cooper and Tobolsky, 1966; Koutsky et al., 1970; Chen-Tsai et al., 1986). For instance, Koutsky et al. (1970) observed a domain size of 3nm~10nm for a polyester-based polyurethane and 5nm~10nm for a polyether-based polyurethane; Chen-Tsai et al. (1986) observed a hard domain length scale of about 11nm with inter-domain distance of 13nm for a PBD/TDI/BD-based polyurethane.

The presence of hard domains in segmented polyurethanes is very important to the

[1] The provider of the sample would prefer the composition of the material unrevealed.

mechanical properties. In segmented polyurethanes, hard domains act as physical crosslinks, playing a role similar to chemical crosslinks in vulcanizates and imparting the material's elastomeric behavior. Since hard domains also occupy significant volume and are stiffer than soft domains, they also function as effective nano-scale fillers and render a material behavior similar to that of a composite (Petrovic and Ferguson, 1991). At room temperature, soft domains are above their glass transition temperature and impart the material its rubber-like behavior; hard domains are below their glassy or melt transition temperature and are thought to govern the hysteresis, permanent deformation, high modulus, and tensile strength. The domain structure also imparts TPUs' versatility in mechanical properties. A wide variety of property combinations can be achieved by varying the molecular weight of the hard and soft segments, their ratio, and chemical type. For instance, TPUs with shore hardness of from 60A to 70D are available (Payne and Rader, 1993). At present, thermoplastic polyurethanes are an important group of polyurethane products because of their advantage in abrasion and chemical resistance, excellent mechanical properties, blood and tissue compatibility, and structural versatility.

Here, the mechanical behavior of a representative TPU is studied in a series of compression tests probing the time-dependent and cyclic loading effects on the large strain deformation behavior. A constitutive model for the observed stress-strain behavior is then developed and compared directly to experimental data.

2 Stress-Strain Behavior

The stress-strain behavior of TPUs demonstrates strong hysteresis, time dependence, and cyclic softening. In this section, a series of uniaxial compression tests are conducted to

quantitatively identify these features.

2.1 Mechanical Test Descriptions

Uniaxial compression tests were conducted using a computer controlled servo-hydraulic single axial test machine, Instron model 1350. The sample material was a thermoplastic polyurethane with durometer hardness value of 92A immediately after production and about 94A after 1 year of shelf life at room temperature. Sheets of material of about 3mm in thickness were cut into cylinders of about 12mm diameter using a die cutter. To eliminate potential buckling, the sample height to diameter ratio was set to be less than 1. In addition, to reduce the contribution of friction due to the interaction with the compression platens, Teflon sheets were placed between the sample and the platens and the initial height/diameter ratio were set to be greater than 0.5.

Specimens were subjected to constant true strain rate loading-unloading cycles and the true stress vs. true strain curve was documented for each test. True strain was defined as the logarithm of the compression ratio determined as the current height over the initial height, where the current height of the sample was monitored during testing using an extensometer. Height measurements were used to form a feedback loop with the actuator to define and control the displacement history such that constant true strain rate conditions were achieved. True stress was obtained by multiplying nominal stress by the compression ratio (Smith, 1974; Petrovic and Ferguson, 1991), assuming the material incompressible[2].

---

[2] Elastomers are generally incompressible. DSC (Differential Scanning Calorimeter) tests on the sample used in this paper showed that the glass transition temperature was about -40°C and the melting

TPU samples exhibited a certain amount of permanent set after each loading-unloading cycle. The dimensions (diameter and height) of the samples were measured after each loading-unloading cycle to ensure that the true stress-true strain curves always started from the new unloaded specimen height for each cycle. The measurement of the dimensions took about 2~3 minutes, including re-positioning the sample on the compression platen and replacing the Teflon sheets whenever necessary.

2.2 Hysteresis

Figure 4 shows the axial compression true stress-true strain behavior of two fresh samples loaded to two different maximum strains, i.e. $\varepsilon_{\max} = 0.5$ and $\varepsilon_{\max} = 1.0$, respectively. The loading curves show an initially stiff response, followed by rollover to a more compliant behavior at a strain of about 0.15, and stiffen again after a strain of 0.70. The unloading paths show a large hysteresis loop with a residual strain. Additional recovery occurred with time after unloading. Residual strains were measured approximately 1 minute after the tests and were found to be $\varepsilon^r = 0.02$ for the $\varepsilon_{\max} = 0.5$ test, and $\varepsilon^r = 0.062$ for the $\varepsilon_{\max} = 1.0$ test.

---

temperature was about 180°C, which confirmed that the sample was in rubbery state at room temperature. It is hence reasonable to assume the Poisson's ratio ν ranges from 0.48 to 0.50. At logarithm compression strain of 0.5, the error in the stress determination due to the incompressible assumption is 2% (ν=0.48) and 1% (ν=0.49); at logarithm compression strain of 1.0, the error is 4% (ν=0.48) and 2% (ν=0.49).

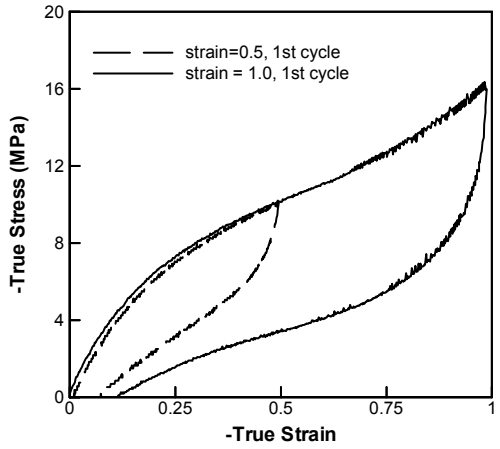

Figure 4: Uniaxial compression tests on fresh samples (N=1) at a strain rate $\dot{\varepsilon} = 0.01/s$, to different maximum strains ($\varepsilon_{\max} = 0.5$ and $\varepsilon_{\max} = 1.0$, respectively). N indicates cycle number.

2.3 Time-Dependence

Figure 5 shows the true stress-true strain curves to $\varepsilon_{\max} = 1.0$ at three different compression strain rates, i.e. $\dot{\varepsilon}_1 = 0.01/s$, $\dot{\varepsilon}_2 = 0.05/s$, and $\dot{\varepsilon}_3 = 0.1/s$. For the loading portions of the curves, the higher the strain rate, the larger the stress. The unloading curves from different strain rate tests are nearly identical, suggesting that unloading behavior has less rate dependence than loading behavior. The residual strains were measured to be $\varepsilon^r = 0.062$ for the $\dot{\varepsilon}_1 = 0.01/s$ test, $\varepsilon^r = 0.046$ for the $\dot{\varepsilon}_2 = 0.05/s$ test, and $\varepsilon^r = 0.043$ for the $\dot{\varepsilon}_2 = 0.1/s$ test.

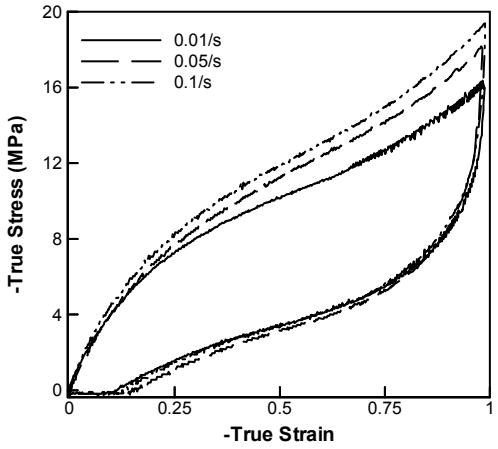

Figure 5: Uniaxial compression tests at three different strain rates.

During the process of loading and unloading, if the test is suspended, time dependence either in the stress response (stress relaxation when the strain is held constant) or in the strain response (creep when the stress is held constant) will be observed for TPUs. Stress relaxation tests were conducted during the course of loading-unloading cycles where the sample was compressed to a maximum strain of 1.0 at a strain rate of 0.1/s with intermittent 60s strain holding periods at strains of 0.2, 0.4, 0.6 and 0.8 during both loading and unloading as shown in the strain history plot of Figure 6(a). Figure 6(b) shows the corresponding true stress-time curve for this test. During each hold period, 50% of stress relaxation occurred in the first 2~5s. During loading, the stress was observed to decrease during the strain hold period; whilst during unloading, the stress was observed to increase during the strain holding period (Figure 6(b,c)). This behavior is characteristic of the time dependent behavior of more conventional elastomeric materials (see, for example, Lion, 1996; Bergstrom and Boyce, 1998).

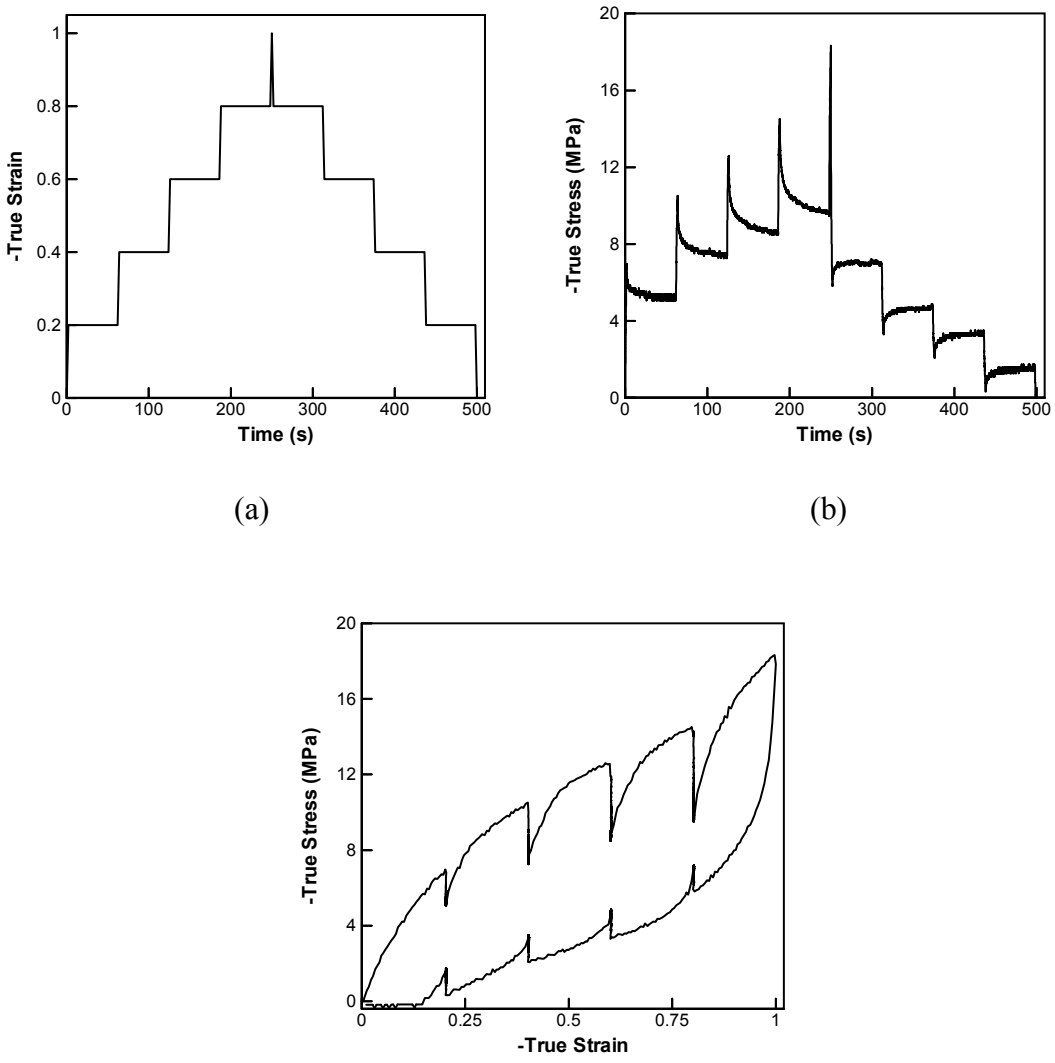

Figure 6: (a) Applied strain history for stress relaxation tests; (b) True-stress vs. time curves for uniaxial compression test with a number of intermittently stops. (c) True-stress vs. true strain curves for the same test.

2.4 Softening

Figure 7 shows the compressive true stress-true strain behavior during the cyclic loading-unloading tests with $\varepsilon_{\max} = 1.0$ and $\dot{\varepsilon} = 0.01/s$. Several features are observed. First, in cyclic tests, the stress-strain curve in the second cycle is far more compliant than that

observed in the first cycle; this effect is referred to as softening behavior. Second, the stress-strain behavior tends to stabilize, after a few cycles, with most softening occurring during the first cycle. Third, as the strain upon reloading approaches the maximum strain achieved in prior cycles, the stress tends to approach the stress level of a first cycle test at that strain. Fourth, the unloading paths after a given strain all follow the same curve, independent of cycle number. Fifth, softening depends upon strain history, where larger strain produces greater softening. Last, the residual strain occurs predominantly after the first cycle, and no significant height changes are observed after the additional cycles. In the rest of this paper, the test whereupon the stress does not show significant decrease from previous cycles will be referred as the stabilized test; stable curves are typically observed after only 4 cycles.

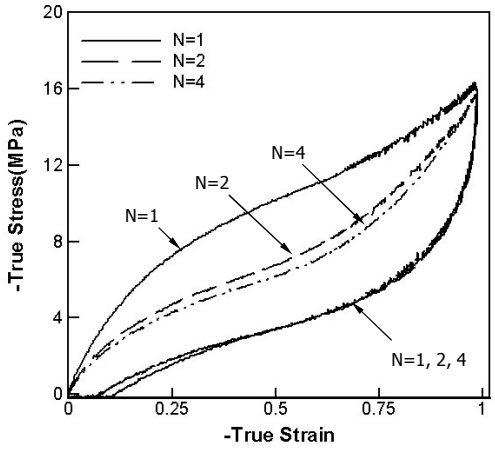

Figure 7: Cyclic uniaxial compression tests at strain rate $\dot{\varepsilon} = 0.01/s$. N indicates cycle number.

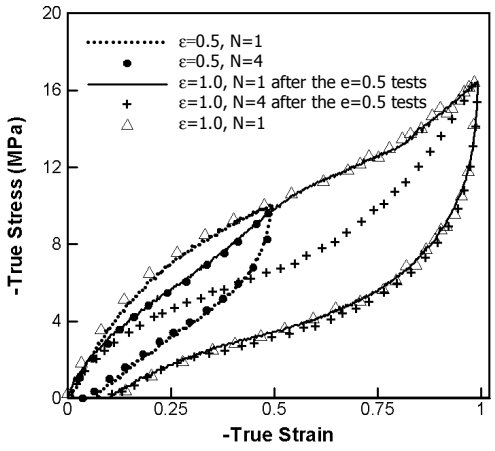

Figure 8: Uniaxial compression tests with cyclic straining to different maximum strains. N indicates cycle number. The strain rate is $\dot{\varepsilon} = 0.01/s$.

Softening was further explored by testing to different cyclic strain magnitudes. Uniaxial compression tests with $\varepsilon_{\max} = 0.5$ and $\varepsilon_{\max} = 1.0$ were conducted on two fresh samples, respectively. The true stress-true strain curves shown earlier in Figure 4 are repeated in Figure 8. The sample strained to $\varepsilon_{\max} = 0.5$ was then subjected to cyclic loading-unloading with $\varepsilon_{\max} = 0.5$. The true stress-true strain curves stabilized after the 4^{th} cycle. This sample was then strained to $\varepsilon_{\max} = 1.0$. As illustrated in Figure 8, upon straining to $\varepsilon_{\max} = 1.0$ after previous excursions to $\varepsilon_{\max} = 0.5$, the true stress-true strain curve for $\varepsilon < 0.5$ moves along the previously stabilized softened curve; as the strain approaches 0.5, the stress approaches the previous maximum stress. After $\varepsilon = 0.5$, the true stress-true strain curve follows the course shown by the fresh sample test with $\varepsilon_{\max} = 1.0$, and the material exhibits the same behavior as the fresh material. The cyclic tests with $\varepsilon_{\max} = 1.0$ result in the stress-strain behavior being softened to the new stabilized curve as defined by $\varepsilon_{\max} = 1.0$ cycle tests on an originally fresh sample. These

variations demonstrate the strong dependence of the material behavior on the strain history as well as characteristic features of cyclic stress-strain behavior.

2.5 Equilibrium Paths

In the stress relaxation tests, the stress relaxes towards an equilibrium state during the holding periods (Figure 6(b)(c) and Figure 9(a)(b)). Figure 9 shows the stress relaxation behavior during the 1st cycle test and during the 4th cycle test after cycling between strains of 0.0 and 1.0. In these tests, the stress relaxes towards two distinct equilibrium paths after 60 seconds for the fresh sample and the cycled sample[3]. The relaxed value at any strain depends upon the maximum strain the material has experienced in its prior loading history. During unloading the increase in stress at each hold period is the same for both the 1st cycle and the 4th cycle tests since both have been strained to a maximum strain of 1.0 before unloading. The stress differences between the stabilized stress from loading vs. unloading hold periods are fairly small for the 4th cycle test. These observations strongly imply that the unloading stress and the loading stress (except the 1st loading) converge to the same equilibrium path, but this path depends on the maximum strain experienced on the loading history. Precisely determining the equilibrium paths for the 1st cycle test and the stabilized test, however, is difficult because of ambiguity in the concept of "long enough time for relaxation". For the first loading, equilibrium paths were determined by finding the point where another 10% stress relaxation would occur at

[3] Further stress relaxation can be expected for a longer relaxation time, but the difference between the two equilibrium paths is so significant that simply accounting for such a difference as the result of insufficient relaxation time is unrealistic.

the same strain. The equilibrium path for the relaxation tests on a previously loaded sample is determined by simply finding the midpoint of the points of the same strains on the loading and the unloading paths of the stabilized test (the 4^{th} cycle test), assuming that the set points under the same strain would converge at their middle points if given infinite time.

Comparing the cyclic tests with $\varepsilon_{\max} = 0.5$ (Figure 4) to those with $\varepsilon_{\max} = 1.0$, we conclude that the softened equilibrium path after cycling at $\varepsilon_{\max} = 0.5$ must be stiffer than the softening equilibrium path after cycling at $\varepsilon_{\max} = 1.0$. Therefore, the degree of softening of the equilibrium path increases with an increase in the prior maximum strain experienced during the overall loading history.

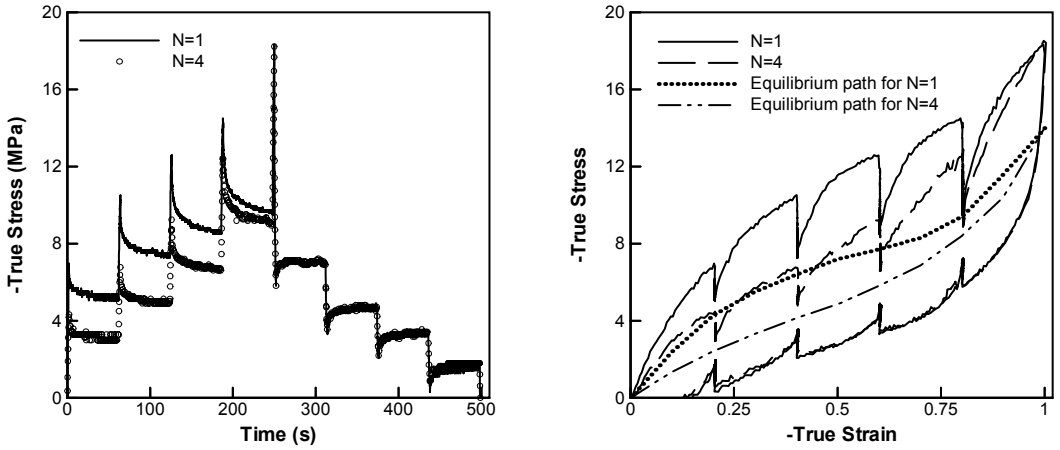

(a) (b)

Figure 9: Uniaxial compression test with a number of intermittent strain hold periods, (a) true-stress vs. time curves, and (b) true-stress vs. true-strain curves and the equilibrium paths for initial and stabilized cycles. N indicates cycle number.

3 Constitutive Model

3.1 A review

A constitutive model for the large strain deformation of TPUs should address the three salient features of the material behavior: 1. Nonlinear large strain elastomeric behavior; 2.Time dependence; 3.Softening of the equilibrium paths observed during cyclic tests.

The experimental data indicates that the stress-strain behavior can be decomposed into a time-independent equilibrium path and a time-dependent departure from the equilibrium path, as illustrated in Figure 10. The constitutive model developed in Boyce et al (2001c) for the stress-strain behavior of thermoplastic vulcanizates (TPVs) is used here as a starting point for the new constitutive model. The equilibrium part of the stress-strain behavior acts as the backbone of the overall material stress-strain behavior and is taken to originate from the entropy change of long molecular chains in the amorphous soft domain due to orientation of the molecular network with deformation. The rate-dependent part is taken to originate from the concomitant internal energy change due to deformation of the hard domains. The viscoplastic response tends to relax the elastic deformation of the hard domains and hence produces the relaxation of the stress-strain behavior to the equilibrium behavior with time. As the strain rate approaches an infinitesimal value, the hard domain elastic deformation will be fully relaxed and the deviation from the equilibrium path will diminish. The viscoplastic behavior comes from energy dissipation sources; potential sources include plastic slip in hard domains, the breakage of hydrogen bonds in the hard domains, possible frictional interaction between two hard domains, and the interaction between the soft and hard domains. In this paper, all energy dissipation mechanisms are lumped into a single viscoplastic constitutive

element.

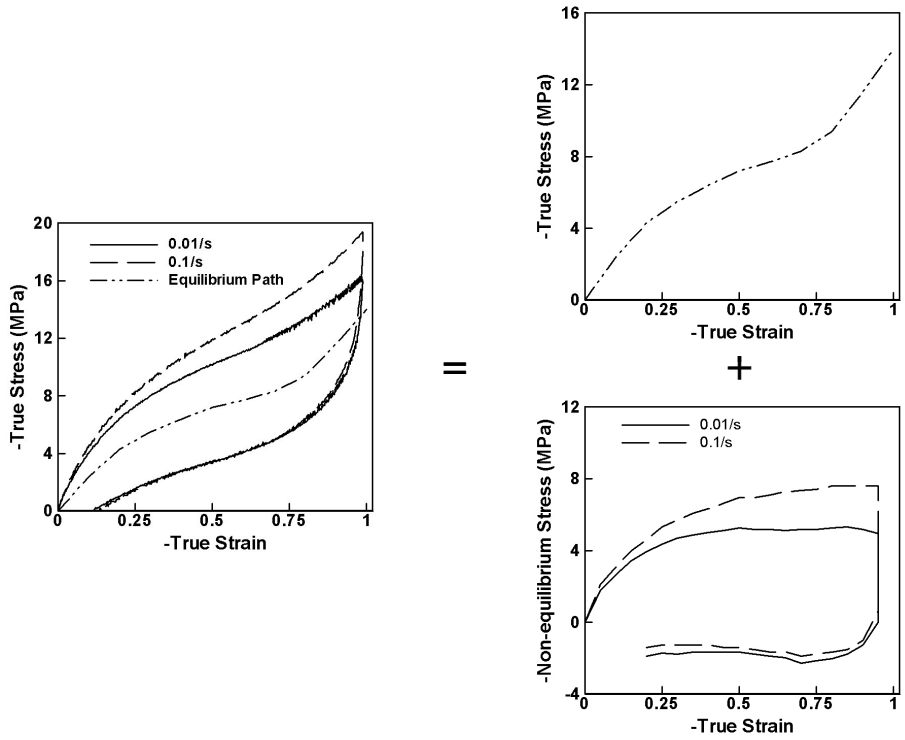

Figure 10: Decomposition of material behavior into a rate-independent equilibrium part and a rate dependent part.

Within this framework of decomposition of material behavior into an equilibrium component and a rate-dependent deviation from equilibrium, we attribute the observed strain history induced softening behavior to be due to softening of the equilibrium path. In rubbery materials, the softening of the equilibrium path is referred to as the "Mullins' effect", so named due to the comprehensive study of this behavior by Mullins on unfilled and filled rubbers during the 1950s and the 1960s (Mullins and Tobin, 1957, 1965; Mullins, 1969).

As demonstrated in the previous section, segmented polyurethanes also demonstrate softening. It is generally believed the domain structure of segmented polyurethane is responsible for the softening, the hysteresis, and the corresponding energy dissipation.

Replacing physical crosslinks in segmented polyurethanes by disrupting the hard domain structure and forming chemical crosslinks was shown to reduce the softening and hysteresis; however, this also resulted in a loss in modulus and tensile strength (Cooper et al. 1976). A number of experimental studies were conducted to investigate the relationship between mechanical properties and material morphology (Bonart, 1968; Bonart et al., 1969; Bonart and Muller-Riederer, 1981; Estes et al., 1971; Kimura et al. 1974; Sauer et al. 2002; Sequela and Prudhomme, 1978; Sung et al., 1979, 1980a, 1980b; Wilkes and Abouzahr, 1981; Yeh et al. 2003;). Bonart and coworkers (Bonart, 1968; Bonart et al., 1969; Bonart and Muller-Riederer, 1981) systematically studied the morphology change during deformation using X-Ray scattering. They and, more recently, Yeh et. al.(2003), found that the stress inhomogeneity in the soft domains could lead to a rotation of the hard domains in order to minimize the overall energy of deformation. They also found that at large stretch the hard domains would break down to further accommodate stretch. Estes and coworkers (1971) found that during tensile deformations the hard domains were displaced into a position where their longer dimensions were predominantly oriented perpendicular to the stretching directions, i.e., a configuration where the hard domains appeared to align perpendicular to the applied stress. To achieve the high degree of hard block orientation, it was necessary that the hard domains underwent plastic deformation, which was accompanied by the breakage and reformation of hydrogen bonds. At sufficiently high strains, the hard domains might break into smaller units.

At present, most elastomer softening theories are based on two concepts. The first theory originates from Blanchard and Parkinson (1952) and Bueche (1960, 1961), who

considered the increase in stiffness produced by fillers to be a result of rubber-filler attachment providing additional restrictions on the crosslinked rubber network. They attributed softening to result from the breakdown or loosening of some of these attachments. Models based on this concept include the works of Bueche (1960, 1961), Dannenberg (1974), and Rigbi (1980), Simo (1987), Govindjee and Simo (1991, 1992), Miehe and Keck (2000), and Lion (1996, 1997). The second theory is due to Mullins, Tobin, Harwood, and Payne (Mullins and Tobin, 1957, 1965; Harwood et al., 1965; Harwood and Payne, 1966a, 1966b; Mullins, 1969), who treated the Mullins' effect as the result of evolution of the microstructure due to a quasi-irreversible rearrangement of molecular networks during deformation. Models based on this concept include Beatty and coworkers (Johnson and Beatty, 1993a, 1993b; Beatty and Krishnaswamy, 2000), Marckmann et al. (2002), and Ogden and coworkers (Ogden and Roxburgh, 1997, 1999; Dorfman and Ogden, 2003; Horgan et al. 2003)(See Qi and Boyce (2004) for a brief discussion on these models.).

In filled elastomers, due to the existence of stiffer fillers, usually carbon black, the strain (or the stretch) is magnified by an amplification factor due to the greater deformation in the soft domains needed to accommodate the applied strain because of the very low strain in the stiffer filler domains. Based on the concept of amplified strain, Mullins and Tobin (1957) suggested that the softening in rubber vulcanizates was due to the decrease of volume fraction of the hard domains with strain, as a result of conversion of the hard domains to the soft domains. Micromechanical modeling of rigid particle filled elastomers by Bergstrom and Boyce (1999) revealed that some of the rubber became trapped among hard particles and could not deform, thus resulting in the effective

fraction of stiff particles to be larger than the physical fraction, so named "occluded volume" effect in filled elastomers postulated by earlier workers (Medalia and Kraus, 1994). In a study of softening in thermoplastic vulcanizates, where the vulcanizates were the fillers, Boyce et al (2001a, 2001b) showed that the cyclic softening was due to the gradual evolution in particle/matrix configuration during previous loading cycles. The plastic deformation of the contiguous thermoplastic phase acted to "release" vulcanizate particles creating a pseudo-continuous vulcanizate phase and thus a softer response during subsequent cycles. Although the material in their study was a system of soft fillers/hard matrix, in contrast to filled rubbers and TPUs, which are hard fillers/soft matrix, their research does enlighten the evolution of the filler/matrix structure with deformation. Based on these observations and Mullins and Tobin concept of an evolution in the underlying hard and soft domain microstructure, we (Qi and Boyce, 2004) recently proposed a new constitutive model to account for the observed softening of the equilibrium stress-strain behavior of elastomer via an evolution in the soft and hard domain structures with stretching. The model was shown to capture stretch-induced softening and is thus used here to represent the softening of the equilibrium behavior of the TPU material.

In this paper, we propose a comprehensive model that captures the observed time dependent nonlinear large strain behavior and softening of the stress-strain behavior. The model is constructed following the decomposition of the material behavior as schematically illustrated in Figure 10 and is detailed in the following.

3.2 Constitutive Model Description

The model requires three constitutive elements, illustrated schematically in Figure 11 for

a one-dimensional rheological analog to the elastomer deformation model. The viscoelastic-plastic component consists of a linear elastic spring characterizing the initial elastic contribution due to internal energy change, and a nonlinear viscoplastic dashpot capturing the rate and temperature dependent behavior of the material. The equilibrium behavior is modeled with the hyperelastic rubbery spring component capturing the entropy change due to molecular orientation of soft domains and is responsible for the high elasticity (large recoverability) of the overall deformation. We note that in the actual material, there are constant interchanges and interplays between deformations in the soft and hard domains. Here, we average out this interplay by taking the two elements to be "in parallel" in the one-dimensional analog which, in turn, corresponds to subjecting both elements (the rubbery spring element and the viscoelastic-plastic elements) to the same deformation in the general three-dimensional case. In the following, superscript N denotes the variables acting on the hyperelastic rubbery network spring, whilst superscript V denotes the variables acting on the viscoelastic-plastic component. Due to the parallel arrangement of these components,

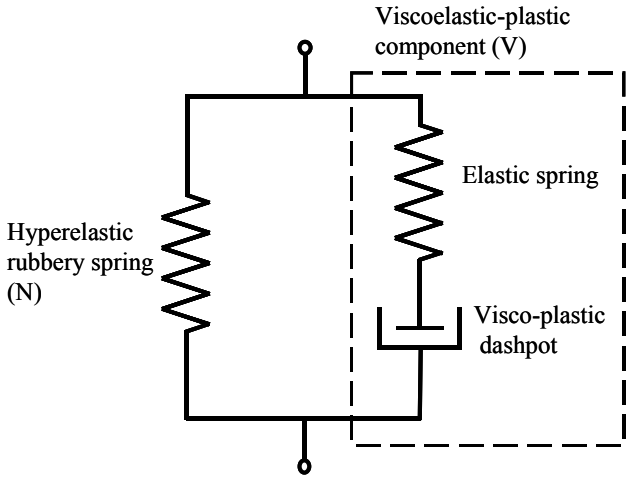

Figure 11: One-dimensional schematics of the constitutive model.

$$\mathbf{F}^N = \mathbf{F}^V = \mathbf{F}, \tag{1}$$

where $\mathbf{F}$ is the macroscopic deformation gradient; $\mathbf{F}^N$ is the deformation gradient acting on the hyperelastic rubbery network, and $\mathbf{F}^V$ is the deformation gradient acting on the viscoelastic-plastic component. The total Cauchy stress is thus given by

$$\mathbf{T} = \mathbf{T}^N + \mathbf{T}^V, \tag{2}$$

where $\mathbf{T}^N$ is the portion of the stress originating from the hyperelastic rubbery behavior; $\mathbf{T}^V$ is the portion originating from the viscoelastic-plastic (hard) domains. The rubbery and viscoelastic-plastic elements each require constitutive models as described below.

3.3 Hyperelastic Rubbery Network Behavior

The stress acting on the hyperelastic rubbery spring, $\mathbf{T}^N$, captures the resistance to entropy change in the soft domains due to molecular network orientation (stretching and alignment), and is modeled using the recent model proposed by Qi and Boyce (2004) to account for the observed stretch-induced softening behavior. Here, the model will be briefly outlined; the detailed description of the model and discussion can be found in Qi and Boyce (2004).

For an isotropic homogeneous elastomer, the Langevin chain based Arruda-Boyce eight-chain model (Arruda and Boyce, 1993) captures the hyperelastic behavior of the material up to large stretch and is used here to represent the equilibrium behavior. Taking the rubbery network strain to be deviatoric, the Arruda-Boyce eight-chain model gives the Cauchy stress as

$$\mathbf{T}^N = \frac{\mu_r}{3J}\frac{\sqrt{N}}{\lambda_{chain}}\mathcal{L}^{-1}\left(\frac{\lambda_{chain}}{\sqrt{N}}\right)\overline{\mathbf{B}}', \tag{3}$$

where $\mu_r = nk\Theta$, k is Boltzmann's constant, Θ is absolute temperature, n is chain

density (number of molecular chains per unit reference volume) of the underlying macromolecular network, and N is the number of "rigid links" between two crosslinks (and/or strong physical entanglements). In this model, $\mathbf{F}^N$ will potentially contain a small volumetric strain[4], which is taken out through $\overline{\mathbf{F}}^N = J^{-1/3}\mathbf{F}^N$ where $J = \det\left[\mathbf{F}^N\right]$. $\overline{\mathbf{B}}$ is the isochoric left Cauchy-Green tensor, $\overline{\mathbf{B}} = \overline{\mathbf{F}}^N\overline{\mathbf{F}}^{NT}$, and $\overline{\mathbf{B}}' = \overline{\mathbf{B}} - \frac{1}{3}tr\left(\overline{\mathbf{B}}\right)\mathbf{I}$ is the deviatoric part of $\overline{\mathbf{B}}$. $\lambda_{chain} = \sqrt{\bar{I}_1/3}$ is the stretch on each chain in the eight-chain network, and $\bar{I}_1 = tr(\overline{\mathbf{B}})$ is the first invariant of $\overline{\mathbf{B}}$. $\mathcal{L}$ is the Langevin function defined as

$$\mathcal{L}(\beta) = \coth\beta - \frac{1}{\beta}. \tag{4}$$

For thermoplastic polyurethane elastomers, the hard domains play an important role in the mechanical properties of thermoplastic polyurethane elastomers. In addition to acting as physical crosslinks imparting material rubbery stress-strain behavior, hard domains occupy a significant volume serving as effective stiff fillers in the material (Petrovic and Ferguson, 1991). This suggests that it is reasonable to model the equilibrium behavior of TPUs using the methodology for elastomer composites where the elastomer is reinforced with very stiff particles. Here, the soft domains are treated as the matrix occupying effective volume fraction v_s, and the hard domains are treated as fillers occupying effective volume fraction v_h. We emphasis that v_s and v_h should be regarded as effective volume fractions and are different from the actual volume fractions

[4] In this comprehensive model, the bulk resistance to volumetric strain (i.e. the bulk modulus) will be lumped into the viscoelastic-plastic component which acts in parallel with the rubbery spring element.

calculated from the material composition of soft and hard segments. This difference will be discussed in more detail following the presentation of the model for the hyperelastic rubbery spring.

In filled elastomers, the average strain (or alternatively, stretch) in the elastomeric domains is necessarily amplified over that of the macroscopic strain since the stiff filler particles accommodate little of the macroscopic strain. For a general three dimensional deformation state, the first invariant of the stretch is amplified by (Bergstrom and Boyce, 1999)

$$\langle I_1 \rangle_m = X\left(\langle I_1 \rangle - 3\right) + 3, \tag{5}$$

where $\langle I_1 \rangle_m$ is the average I_1 in the matrix, and $\langle I_1 \rangle$ is the overall macroscopic I_1 of the composite material, and X is an amplification factor dependent on particle volume fraction, v_f, and distribution. X can take a general form of $X = 1 + 3.5v_f + bv_f^2$. Here, we further choose $X = 1 + 3.5(1 - v_s) + 18(1 - v_s)^2$ to characterize a well-dispersed composite system where v_s is the soft domain volume fraction.

Following Bergstrom and Boyce(2000) and Qi and Boyce(2004), the Cauchy stress as modified by amplified strain is given by:

$$\mathbf{T}^N = \frac{v_s X \mu}{3J} \frac{\sqrt{N}}{\Lambda_{chain}} \mathcal{L}^{-1}\left(\frac{\Lambda_{chain}}{\sqrt{N}}\right) \overline{\mathbf{B}}', \tag{6}$$

where Λ_{chain} is the amplified chain stretch defined as $\Lambda_{chain} = \sqrt{X\left(\lambda_{chain}^2 - 1\right)^2 + 1}$ and $X = 1 + 3.5(1 - v_s) + 18(1 - v_s)^2$.

In a TPU, the effective volume fraction v_s of the soft domains is not equal to the volume fraction of soft segments calculated from the material chemistry. On the one

hand, phase separation in TPUs is generally incomplete and there exist isolated hard segments, resulting in a smaller volume fraction of the hard domains than that obtained from composition calculation; on the other hand, a portion of the soft domains is occluded by the hard domains, resulting in an increase in the effective hard domain volume fraction. The latter will dominate the small to middle deformation, whereas the first causes the effective soft domain volume fraction to possibly become larger than the segment composition calculation at large deformations when all of the soft domain has been released from occlusion and isolated hard segments may resolve in soft domains. Following Qi and Boyce (2004), we take v_s to evolve with deformation where initially occluded regions of soft domains are gradually released with deformation and this evolution is driven by the local chain stretch, Λ_{chain}, in the soft domains. Upon removal of applied load, it was found that the hard domains remained largely in the deformed configuration with very little recovery (Estes et al. 1971). We thus assume that the configuration change of the hard domains is taken to be permanent. Therefore, we take v_s to remain at its value attained at the maximum chain stretch $\Lambda_{chain}^{\max}$ encountered during its loading history. Evolution in v_s will be re-activated as the local chain stretch exceeds the previous maximum chain stretch. Therefore, when $\Lambda_{chain} > \Lambda_{chain}^{\max}$, v_s is modeled to increase with increasing Λ_{chain}, and thus the amplification X decreases with increasing Λ_{chain}. We also assume v_s varies from an initial value v_{s0} to a saturation value v_{ss} as the local chain stretch Λ_{chain} reaches the locking stretch of the chain, $\lambda_{chain}^{locking}$. The evolution of v_s is taken to obey the following rule:

$$\dot{v}_s = A(v_{ss} - v_s)\frac{\lambda_{chain}^{lock} - 1}{\left(\lambda_{chain}^{lock} - \Lambda_{chain}^{\max}\right)^2}\dot{\Lambda}_{chain}^{\max}, \tag{7a}$$

where

$$\dot{\Lambda}_{chain}^{\max} = \begin{cases} 0 & , \quad \Lambda_{chain} < \Lambda_{chain}^{\max} \\ \dot{\Lambda}_{chain} & , \quad \Lambda_{chain} \geq \Lambda_{chain}^{\max} \end{cases}, \tag{7b}$$

and A is a parameter that characterizes the evolution in v_s with increasing Λ_{chain}. (For a discussion on this evolution rule and its effect on the Cauchy stress, see Qi and Boyce (2004).)

3.4 Viscoelastic-plastic Element

The stress contribution from the viscoelastic-plastic component, $\mathbf{T}^V$, is given by

$$\mathbf{T}^V = \frac{v_h}{\det \mathbf{F}^{Ve}}\mathbf{L}^e\left[\ln \mathbf{V}^{Ve}\right], \tag{8}$$

where $\mathbf{L}^e$ is the fourth-order tensor modulus of elastic constants; $\mathbf{F}^{Ve}$ is the elastic deformation gradient and $\mathbf{V}^{Ve}$ is the left stretch tensor of the elastic deformation gradient obtained from the polar decomposition $\mathbf{F}^{Ve} = \mathbf{V}^{Ve}\mathbf{R}^{Ve}$, where $\mathbf{R}^{Ve}$ is the rotation tensor. v_h is the effective volume fraction of hard domains. It should be noted that a TPU is not a composite material, even though a methodology for composite material averaging is used here. Since the viscoelastic-plastic component captures a significant portion of the initial elastic stiffness of the material and lumped energy dissipation, the combination of these behaviors is believed to relate to the hard domain and soft-hard domain interactions. We simply take $v_h = 1 - v_s$.

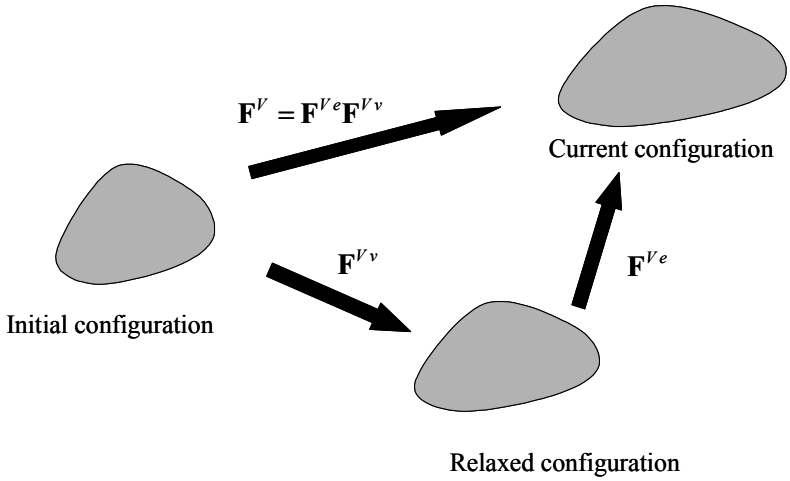

Figure 12: Schematic of decomposition of $\mathbf{F}^V$ into elastic and visco-plastic parts.

The elastic deformation gradient is determined from the multiplicative decomposition of $\mathbf{F}^V$ into elastic and viscoplastic contributions (Figure 12)

$$\mathbf{F}^V = \mathbf{F}^{Ve}\mathbf{F}^{Vv}. \tag{9}$$

where $\mathbf{F}^{Vv}$ is in a relaxed configuration obtained by elastic unloading. The corresponding decomposition of the velocity gradient is

$$\mathbf{L}^V = \dot{\mathbf{F}}^V\mathbf{F}^{V-1} = \dot{\mathbf{F}}^{Ve}\mathbf{F}^{Ve-1} + \mathbf{F}^{Ve}\dot{\mathbf{F}}^{Vv}\mathbf{F}^{Vv-1}\mathbf{F}^{Ve-1}. \tag{10}$$

The velocity gradient of the relaxed configuration is given by

$$\mathbf{L}^{Vv} = \dot{\mathbf{F}}^{Vv}\mathbf{F}^{Vv-1} = \mathbf{D}^{Vv} + \mathbf{W}^{Vv}, \tag{11}$$

where $\mathbf{D}^{Vv}$ and $\mathbf{W}^{Vv}$ are the rate of stretching and the spin, respectively. We take $\mathbf{W}^{Vv} = \mathbf{0}$ with no loss in generality as shown in Boyce et al (1988). The visco-plastic stretch rate $\mathbf{D}^{Vv}$ is constitutively prescribed to be

$$\mathbf{D}^{Vv} = \frac{\dot{\gamma}^v}{\sqrt{2}\bar{\tau}_V}\overline{\mathbf{T}}^{V\prime}, \tag{12}$$

where $\overline{\mathbf{T}}^V$ is the stress acting on the viscoelastic-plastic component convected to its

relaxed configuration ($\overline{\mathbf{T}}^{V} = \mathbf{R}^{Ve^T}\mathbf{T}^{V}\mathbf{R}^{Ve}$); the prime denotes the deviator; $\bar{\tau}_V$ is the equivalent shear stress and

$$\bar{\tau}_V = \left[\frac{1}{2}\overline{\mathbf{T}}^{V'} \bullet \overline{\mathbf{T}}^{V'}\right]^{1/2}. \tag{13}$$

$\dot{\gamma}^v$ denotes the visco-plastic shear strain rate of the viscoplastic component, and is constitutively prescribed to take the form

$$\dot{\gamma}^v = \dot{\gamma}_0 \exp\left[-\frac{\Delta G}{k\Theta}\left\{1-\left(\frac{\bar{\tau}_V}{s}\right)\right\}\right], \tag{14}$$

where $\dot{\gamma}_0$ is the pre-exponential factor proportional to the attempt frequency, ΔG is the zero stress level activation energy, and s is the athermal shear strength, which represents the resistance to the visco-plastic shear deformation in TPUs.

The true stress-true strain behavior including relaxation periods (Figure 9) shows that the amount of stress decrease during loading strain hold periods is larger than the amount of stress increase during unloading strain hold periods. This effect is significant during the 1st cycle test. This suggests the resistance to viscous flow evolves with strain history. Although the mechanism is not clear yet, a possible conjecture is that such a mechanism change is related to the configuration change of soft and hard domains as evidenced by Estes et al (1971). During the loading course, the hard domain clusters will irreversibly change their configuration to accommodate local deformation by breaking and reforming the hydrogen bonds. We propose the following evolution rule as a first step to capture this behavior,

$$s_1 = \left(\frac{v_h}{v_{h0}}\right)s_0. \tag{15}$$

3.5 Summary of the Constitutive Model

The deformation behavior of a TPU is not trivial. It is highly nonlinear; it is rate dependent; it is hysteretic; and it softens with cyclic loading where the degree of softening depends on the maximum strain level reached in prior cycles. The new constitutive model is summarized in Table 1 where the material parameters needed to fully capture each feature of the deformation behavior are listed.

Due to the ability to systematically break down the stress-strain behavior, a systematic procedure for determining values for the material properties can be developed. The three constitutive elements in the model each account for different features of the observed material behaviors: i.e. the hyperelastic rubbery softening spring for equilibrium behavior; the evolution of effective volume fraction of soft domains for the softening of equilibrium paths; the linear elastic spring accounting for the stiffness contribution of the time dependent behavior; and the viscoplastic dashpot accounting for the nonlinear time dependent behavior. It is thus possible to identify the material parameters associated with the different features of the material behavior. The Appendix provides a methodology to identify the material parameters.

Table 1. Summary of constitutive model and material parameters.

$\mathbf{T} = \mathbf{T}^N + \mathbf{T}^V$	Equilibrium Stress-Strain Response $\mathbf{T}^N$	Hyperelastic Rubbery Spring Element	Hyperelastic "filler" effect	μ_r, N,	$\mathbf{T}^N = \frac{v_s X \mu}{3J} \frac{\sqrt{N}}{\Lambda_{chain}} \mathcal{L}^{-1}\left(\frac{\Lambda_{chain}}{\sqrt{N}}\right)\overline{\mathbf{B}}'$ $X = 1 + 3.5(1 - v_s) + 18(1 - v_s)^2$
			Softening	v_{s0}, v_{ss}, A	$v_s = v_{ss} - (v_{ss} - v_{s0})\exp\left(-A\frac{\Lambda_{chain} - 1}{\lambda_{chain}^{lock} - \Lambda_{chain}}\right)$
	Non-equilibrium Rate Dependent Stress-Strain Response $\mathbf{T}^V$	Linear Spring Element		E_v, ν	$\mathbf{T}^V = \frac{v_h}{\det \mathbf{F}^{Ve}} \mathbf{L}^e \left[\ln \mathbf{V}^{Ve}\right]$ $v_h = 1 - v_s$
		Viscoplastic Dashpot Element	Time Dependence	$\dot{\gamma}_0$, ΔG	$\dot{\gamma}^v = \dot{\gamma}_0 \exp\left[-\frac{\Delta G}{k\Theta}\left\{1 - \left(\frac{\bar{\tau}_V}{s}\right)\right\}\right]$
			Softening	s_0,	$s = \left(\frac{v_h}{v_{i0}}\right) s_0$

4 Results

The material parameters for the TPU tested in this study were identified using the procedure outlined in the Appendix and are listed in Table 2.

Table 2: Material parameters.

Stretch Softening Hyperelastic Rubbery Spring				
μ_r	N	A	v_{s0}	v_{ss}
(MPa)				
1.40	6.0	1.4	0.4	0.8

Elastic-Viscoplastic Component				
Linear Elastic Spring		Viscoplastic Dashpot		
E_v	ν	s_0	$\dot{\gamma}_0$	ΔG
(MPa)		(MPa)	(10^{-2})	$(10^{-20} J)$
51	0.48	2.21	1.94	1.31

Uniaxial compression tests at different constant strain rates on fresh samples were simulated to verify the proposed constitutive model. Figure 13(a) shows the simulation and experimental stress-strain curves for the tests at $|\dot{\varepsilon}| = 0.01 s^{-1}$ and $|\dot{\varepsilon}| = 0.1 s^{-1}$. The simulation results agree very well with the experimental data and capture the rate dependence of the stress strain behavior. Figure 13(b) shows the decomposition of the material stress-strain behavior into an equilibrium part (same for both strain rates) and a time dependent part, illustrating the methodology of material behavior decomposition. The proposed model does not fully capture the feature that the unloading curves follow

the same path for the tests at different strain rates, but the difference is small. Further improvement in the overall unloading behavior can be achieved by allowing a small amount of time prior to unloading. Figure 14 shows the true stress-true strain curve from the simulation when a 30 second delay was allotted prior to unloading.

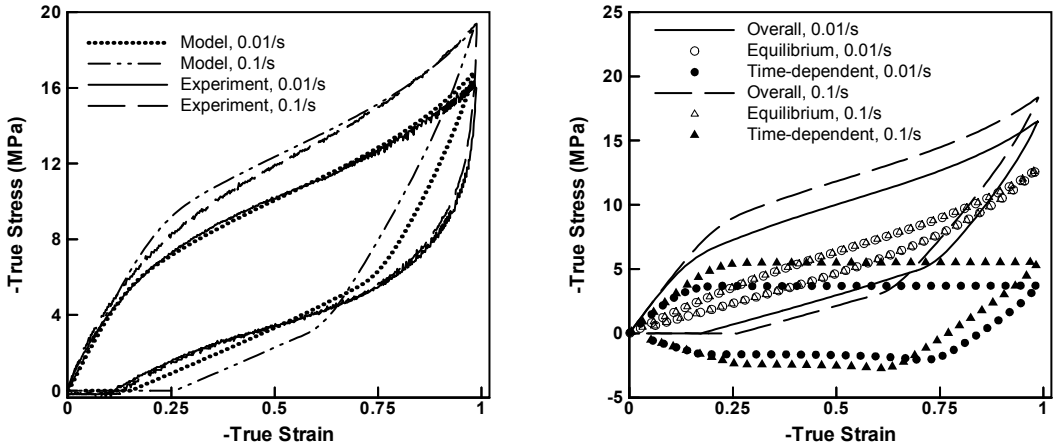

(a) (b)

Figure 13: (a) True Stress-true strain curves for uniaxial compression tests; (b) Decompositions of the stress-strain behavior into an equilibrium part and a time dependent part.

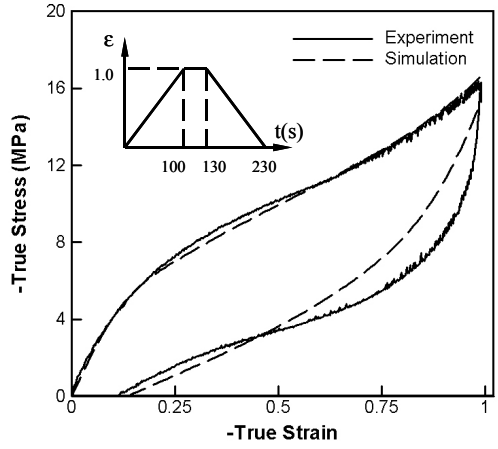

Figure 14: True Stress-true strain curves for uniaxial compression test with $\dot{\varepsilon} = 0.01/s$ and 30 seconds delay before unloading. The inset shows the true strain loading history.

Simulations on cyclic loading-unloading tests were also conducted. Recall that the TPU sample showed residual strain (permanent set) after unloading. In the experiments, the dimensions of the sample (diameter and height) were measured between cycles, and were used as the new dimension for the sample so that the true stress-true strain curves always started from the new unloaded specimen height for each cycle. Such a process of having the true stress-true strain curve begin at the origin by measuring the dimensions before each test corresponds to simply shifting the true stress-true strain curves leftward by the amount of residual strain ε^r. In simulations, the true stress-true strain curves were first obtained based on the initial dimensions of the sample and were then shifted leftward by the residual strain measured after 2 minutes idling time between the two cyclic simulations, so chosen corresponding to the 2 minute period between cycles used to measure the dimension change and reposition the sample on the platen for the next cycle of loading. Figure 15(a) shows the loading history for the test with $\varepsilon_{\max} = 1.0$ and $|\dot{\varepsilon}| = 0.1 s^{-1}$. Due to the shift of the curve, the second cycle simulation was loaded to the strain $1+\varepsilon^r$, where ε^r is the residual strain measured from the first cycle simulation.

Simulations on cyclic loading-unloading tests were conducted at a strain rate of $|\dot{\varepsilon}| = 0.01 s^{-1}$ (Figure 15(b)) and $|\dot{\varepsilon}| = 0.1 s^{-1}$ (Figure 15(c)). The model captures the loading and unloading paths at both strain rates. The residual strain after 2min idling time in the simulation was 0.05, which was very close to the residual strain of 0.04~0.06 observed in the experiments. Figure 15(d) and (e) show the decomposition of the material stress-strain behavior into an equilibrium part and a time dependent part for each cycle of the tests. From Figure 15(d) and (e), the equilibrium parts during loading and unloading for the second cycle follow the same path, indicating that additional softening does not

occur during the second loading cycle.

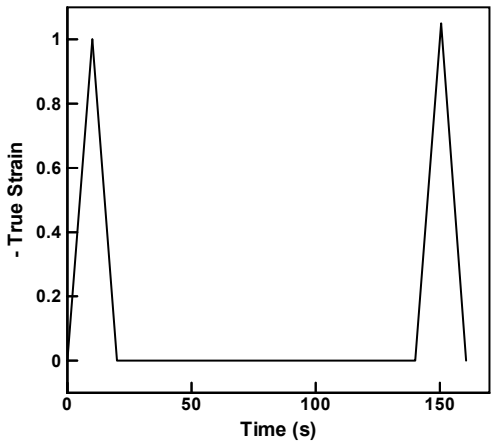

(a)

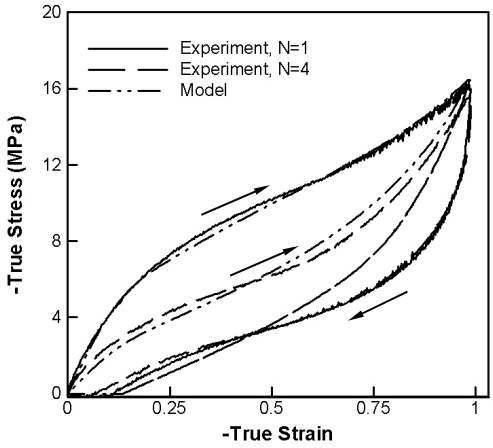

(b)

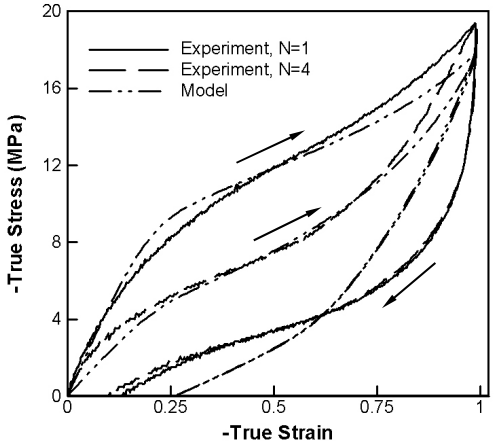

(c)

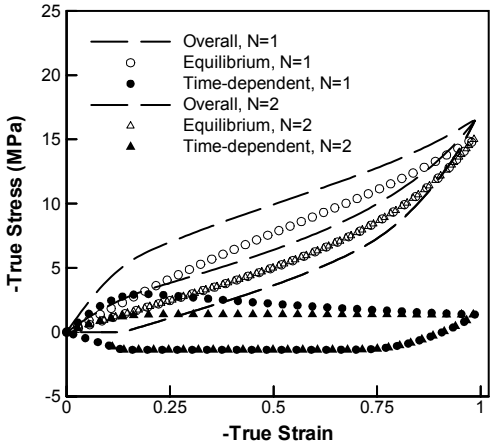

(d)

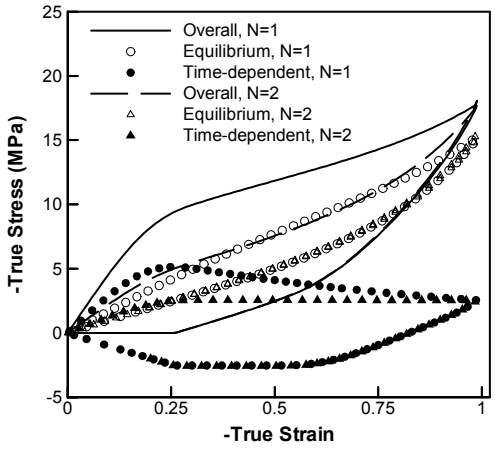

(e)

Figure 15: Numerical simulation on cyclic loading tests: (a) loading history; Stress-strain behavior for (b) $\dot{\varepsilon} = 0.01/s$; and (c) $\dot{\varepsilon} = 0.1/s$; Decompositions of the stress-strain behavior into an equilibrium part and a time dependent part for (d) $\dot{\varepsilon} = 0.01/s$; and (e) $\dot{\varepsilon} = 0.1/s$. N indicates cycle number.

Figure 16(a) shows the cyclic loading to different maximum strains at $\dot{\varepsilon} = 0.01/s$ where the sample was subjected to three loading-unloading cycles: the first cycle was loaded to $\varepsilon_{\max} = 0.05$, and the second and the third cycles were loaded to $\varepsilon_{\max} = 1.0$. The corresponding experimental results are also presented in the figure. The numerical simulations adequately capture the softening effects during the cyclic tests. It is noted that the experimental results used to obtain material parameters did not include the tests with loading to $\varepsilon_{\max} = 0.5$, but the model predicts the softening response corresponding to 0.5 strain. Figure 16(b) shows the evolution of the effective volume fraction of soft domain during this deformation course. The v_s evolves with strain from the original $v_{s0} = 0.4$ and reaches $v_s = 0.59$ at $\varepsilon_{\max} = 0.5$. This value for v_s is retained until the strain exceeds 0.5 upon reloading, whereupon v_s starts increasing again.

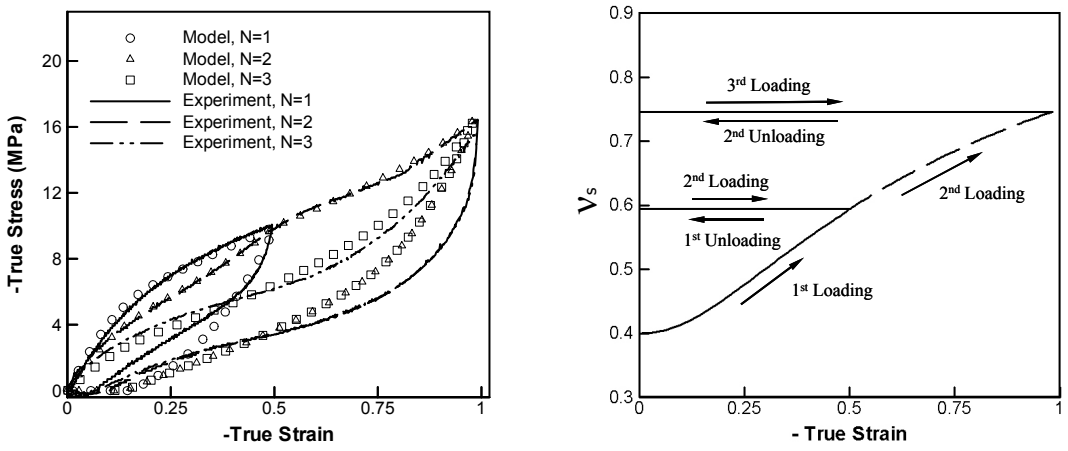

(a) (b)

Figure 16**:** Cyclic loading to different maximum strains, i.e. $\varepsilon = 0.5$ first, then $\varepsilon = 1.0$ with strain rate of $\dot{\varepsilon} = 0.01/s$. (a) true stress-true strain curve; (b) evolution of effective volume fraction of soft domain. For both simulations and experiments, the curves are the first loading to $\varepsilon = 0.5$ then unloading (N=1), followed by reloading to $\varepsilon = 1.0$ then unloading (N=2), finally reloading to $\varepsilon = 1.0$ then unloading (N=3). In experiments, the subsequent reloading occurred after the stress-strain behavior stabilized.

Figure 17 shows the numerical simulation of the relaxation test at $\dot{\varepsilon} = 0.1/s$. For the first cycle (Figure 17(a)), the numerical simulation captures the decrease/increase of the stress during each hold period during loading/unloading, except for the stop at $\varepsilon = 80\%$ during unloading due to relative slow stress drop at the transition from loading to unloading in the simulation. Figure 17(c) and (d) show the one-dimensional decomposition of the material stress-strain behavior into an equilibrium part and a time dependent part for each cycle of the tests.

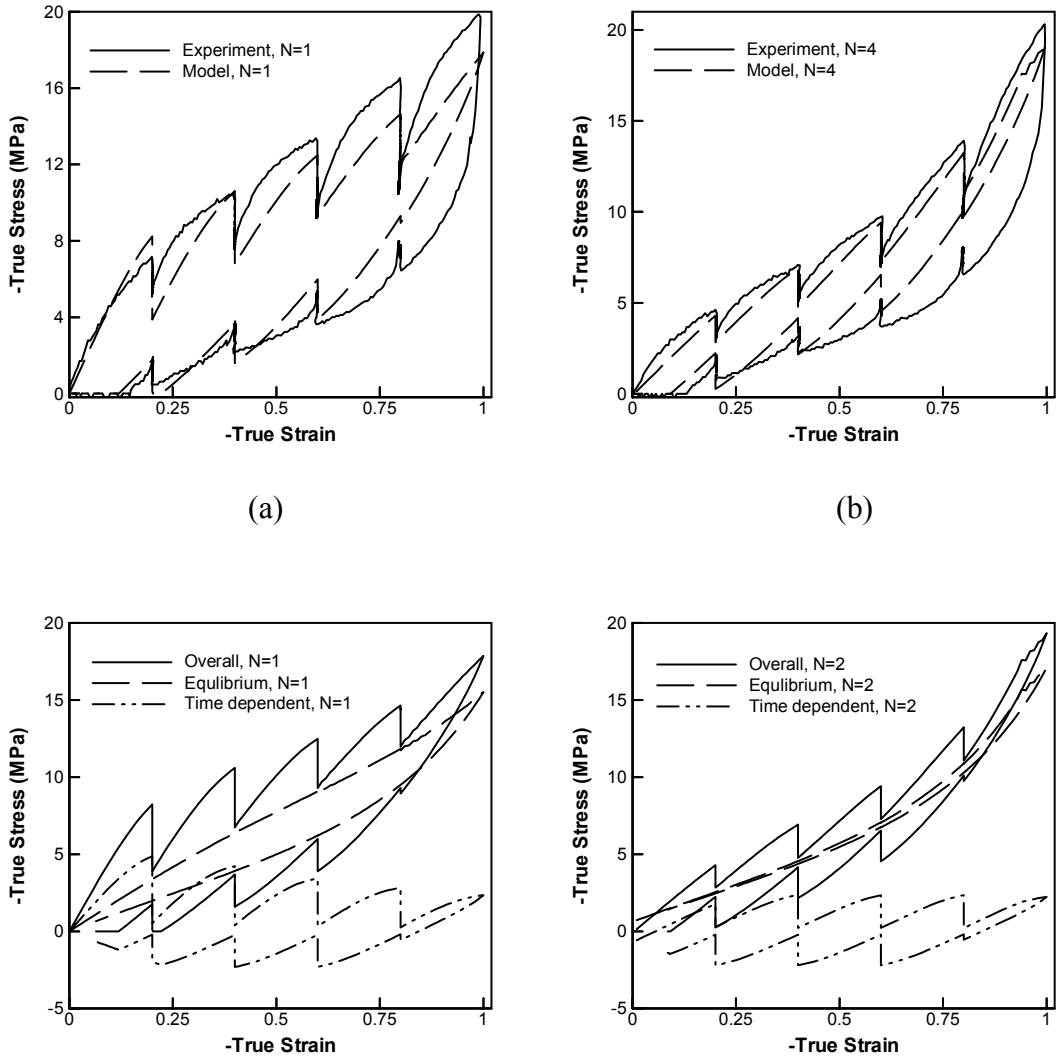

Figure 17: Numerical simulations of relaxation test: (a) the 1st cycle; (b) the 2nd cycle curves; Decomposition the material stress-strain behavior into an equilibrium part and a time dependent part: (c) the 1st cycle; (d) the 2nd cycle curves. N indicates cycle number.

5 Conclusion

The large strain stress-strain behavior of thermoplastic polyurethane was investigated in this paper. It was shown by uniaxial compression tests that TPUs exhibited very complicated stress-strain behavior, which has strong rate dependence, hysteresis, and

softening, where the softening is evident upon reloading. A set of experiments has been presented which acted to isolate these various dependencies and features of the stress-strain behavior. In seeking a constitutive that can be applied to general 3-dimensional engineering analysis, such a complicated behavior impedes any attempts at a simple phenomenological curve-fit model and dictates the need for a physically-based constitutive model.

A constitutive model accounting for the rate dependent hysteresis behavior of polyurethane materials and the softening behavior is then presented. The constitutive model decomposes the material behavior into a rate-independent equilibrium part and a rate-dependent viscoelastic-plastic part. For the softening of the equilibrium path, the model adopts the concept of amplified strain, and takes the strain amplification factor to evolve with loading history due to microstructural reorganization of the soft and hard domains which act to increase the volume fraction of the effective soft domain. Comparisons of numerical simulations of uniaxial compression tests with experimental data verify the proposed constitutive model. The model adequately captures the overall nonlinear behavior, the softening (Mullins' effect), and the time dependent behavior of the TPUs.

The underlying material structure of TPUs undergoes significant changes during large deformation. As a first approach, these changes are emulated in the proposed constitutive model by simply taking the volume fraction of the soft domain to evolve with deformation. However, structural changes will also alter other structure-dependent processes such as the time-dependent viscous response and will result in anisotropy of the structure and behavior. The underlying physical process for these evolution rules is not

clear. In the future, micromechanical modeling, together with advanced experiments whereby structural evolution is monitored with deformation, should be used to explore these important aspects.

Appendix: Parameter Identification for the Constitutive Model

In order to identify the material parameters in the proposed constitutive model, two types of cyclic tests are necessary: Cyclic relaxation tests (tension or compression) with intermittent holding period at distinct strains during both loading and unloading courses to identify equilibrium stress-strain response of the material; cyclic tests (tension or compression) at different strain rates to identify rate-dependent behavior of the materials. Here, the procedure of parameter identification is exemplified using the cyclic uniaxial compression tests and relaxation tests described above.

A.1 Material Parameter Identification for Hyperelastic Rubbery Softening Spring

The material parameters associated with the hyperelastic rubbery component of the constitutive model can be determined using the two equilibrium paths (the 1st cycle test and the 4th cycle test after cyclic loading to a strain of 1.0) presented in Figure A1. The initial Young's moduli for these two curves were measured from the initial slopes of the curves, $E_r^{(0)} \approx 24MPa$ and $E_r^{(1)} \approx 14MPa$, where $E_r^{(0)}$ denotes the initial Young's modulus for the 1st cycle equilibrium path, and $E_r^{(1)}$ denotes the initial Young's modulus for the stabilized equilibrium path after a maximum cyclic strain of 1.0. In the following, a superscript 0 denotes the variables for the 1st cycle equilibrium path, and a superscript 1 denotes the variables for the stabilized equilibrium path. The ratio is $E_r^{(0)} / E_r^{(1)} = 1.7$, and

from eqn.(6),

$$\frac{E_r^{(0)}}{E_r^{(1)}} = \frac{v_{s0}X^{(0)}}{v_s^{(1)}X^{(1)}} = \frac{v_{s0}\left[1+3.5(1-v_{s0})+18(1-v_{s0})^2\right]}{v_s^{(1)}\left[1+3.5(1-v_s^{(1)})+18(1-v_s^{(1)})^2\right]} \qquad \text{(A1)}$$

where $v_s^{(1)}$ is effective volume fraction of soft domain at $\varepsilon = 1.0$, and remains constant during the 4th cycle test.

The chemical composition of the TPU used in the current study is 57% soft segment and 43% hard segment. Therefore, based on the argument in the discussion of the effective volume fraction, it is reasonable to assume that $v_{s0} = 0.4$ and $v_{ss} = 0.8$. From eqn. (A1), $v_s^{(1)} \approx 0.75$, $X^{(0)} = 9.58$ and $X^{(1)} = 3.00$.

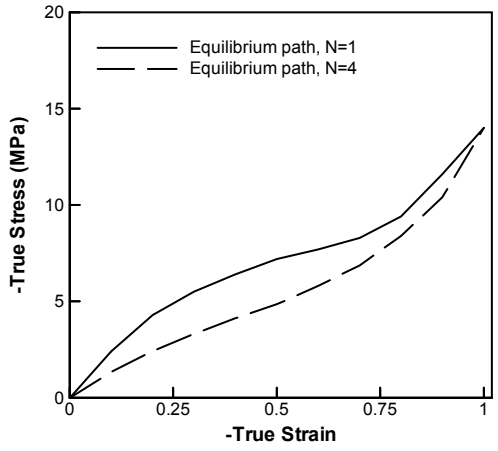

Figure A1: Equilibrium paths from the 1st relaxation test and the 4th relaxation test. N indicates cycle number.

Since in the 4th cycle test, both v_s and X remain constant, it is convenient to use the stabilized equilibrium path to determine parameters μ_r and N in the Arruda-Boyce model. We found $\mu_r = 1.40MPa$ and $N = 6.0$. The locking chain stretch hence is $\lambda_{chain}^{locking} = \sqrt{N} = 2.45$.

In a uniaxial compression test, the compression ratio in the axial direction is λ_1 and is related with compression strain ε by $\lambda_1 = e^{-\varepsilon}$. Assuming material is incompressible, the lateral stretch ratios are $\lambda_2 = \lambda_3 = \sqrt{1/\lambda_1}$. Then the macroscopic equivalent stretch is

$$\lambda_{chain} = \sqrt{\frac{\lambda_1^2 + \lambda_2^2 + \lambda_3^2}{3}} = \sqrt{\frac{e^{-2\varepsilon} + 2e^{\varepsilon}}{3}} \approx \sqrt{\frac{2e^{\varepsilon}}{3}} \qquad \text{(A2)}$$

For $\varepsilon = 1.0$, $\lambda_{chain} \approx 1.35$. The amplified chain stretch ratio is thus $\Lambda_{chain} = 1.86$. From eqn.(7), we obtained $A \approx 1.4$.

Figure A2 shows the curve fitting using the estimated parameters

$$\mu_r = 1.40MPa,\ N = 6.0,\ A = 1.4,\ v_{s0} = 0.4,\ v_{ss} = 0.8.$$

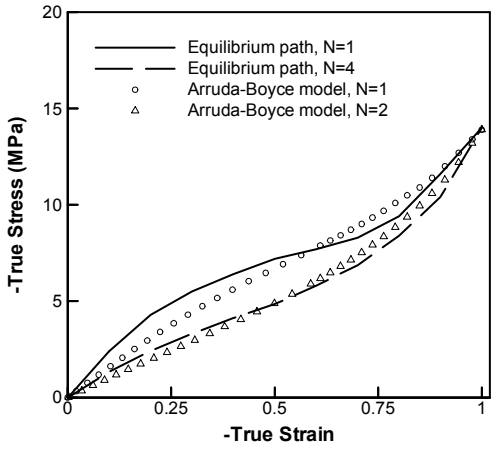

Figure A2: Material parameter identification for the rubbery hyperelastic spring. N indicates cycle number.

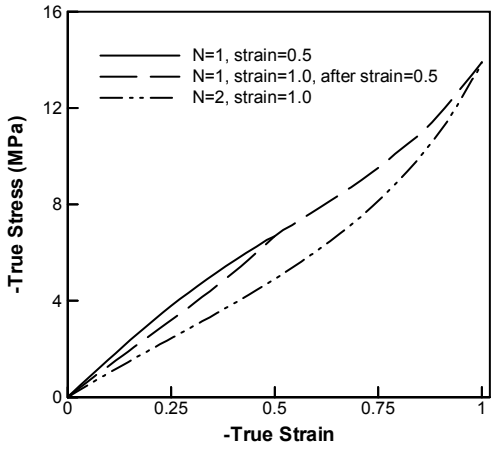

Figure A3: The stress-strain behavior of equilibrium behavior during cyclic loadings to a maximum strain of 0.5 for first cycle, then reloading to 1.0 for two cycles. N indicates cycle number.

The obtained parameters for the equilibrium path were used to simulate the tests where the sample was subjected to three load-unloading cycles: the first one to a maximum strain of 0.50, whereas the last two to a maximum strain of 1.0. Figure A3 shows the numerical simulations. Clearly, the loading to the maximum strain of 0.50 shows less softening in the stress-strain behavior than that with the maximum strain of 1.0.

A.2 Material Parameter identification for viscoelastic-plastic component

From the one dimension simplification of eqn.(2), the axial stress acting on the viscoelastic-plastic component T^V is determined by

$$T^V = T - T^N . \qquad \text{(A3)}$$

The elastic modulus E_v for the elastic spring in the viscoelastic-plastic component can be determined since the initial Young's modulus of the material is the summation of the contributions from hyperelastic rubbery spring and the elastic spring. The initial overall

Young's modulus was measured from the true stress-true strain curve in Figure 7, $E \approx 55MPa$. Hence, $\nu_{h0}E_v = E - E_r \approx 31MPa$, where $\nu_{h0} = 1 - v_{s0}$. Therefore $E_v \approx 51MPa$. Poisson's ratio was chosen as $\nu = 0.48$ to ensure small material compressibility.

For the material parameters associated with the viscoplastic dashpot element, s_0, ΔG, and $\dot{\gamma}_0$ can be determined using the loading curve. From eqn.(A3), T^V vs ε plots for the tests at difference strain rates were constructed, as shown in Figure A4(a).

The equivalent shear strain γ and shear stress τ are related to strain and stress in uniaxial compression tests by

$$\gamma = \sqrt{3}\varepsilon,\ \tau = \frac{1}{\sqrt{3}}T^V \tag{A4}$$

The equivalent visco-plastic shear strain is obtained by subtracting the elastic shear deformation from the total equivalent shear strain

$$\gamma^v = \gamma - \tau / G, \text{ where } G \approx E_v / 3 \tag{A5}$$

The equivalent visco-plastic shear stress and shear strain curves at different strain rate hereby were constructed for the loading path (Figure A4(b)).

Eqn.(14) describes the viscoplastic flow rate and can be rewritten as

$$\tau = c \ln \dot{\gamma}^v + b, \tag{A6}$$

$$c = \frac{s}{D},\ b = \frac{s}{D}\left(D - \ln \dot{\gamma}_0\right),\ D = \frac{\Delta G}{k\Theta}. \tag{A7}$$

Eqn. (A6), together with Figure A4(b), provides insight into the evolution of s during deformation. Indeed, a detailed evolution rule for s can be identified by constructing τ vs $\dot{\gamma}^v$ curves at a number of γ^v from Figure A4(b), and then investigating the variation of

the slopes and interception of the curves with respect of γ^v. Here, for the sake of brevity, we assume s evolves with effective volume fraction of hard domain, i.e. $s = (v_h / v_{h0}) s_0$. As shown in the results, such simplification generally can give good predictions of the stress-strain behavior of the material.

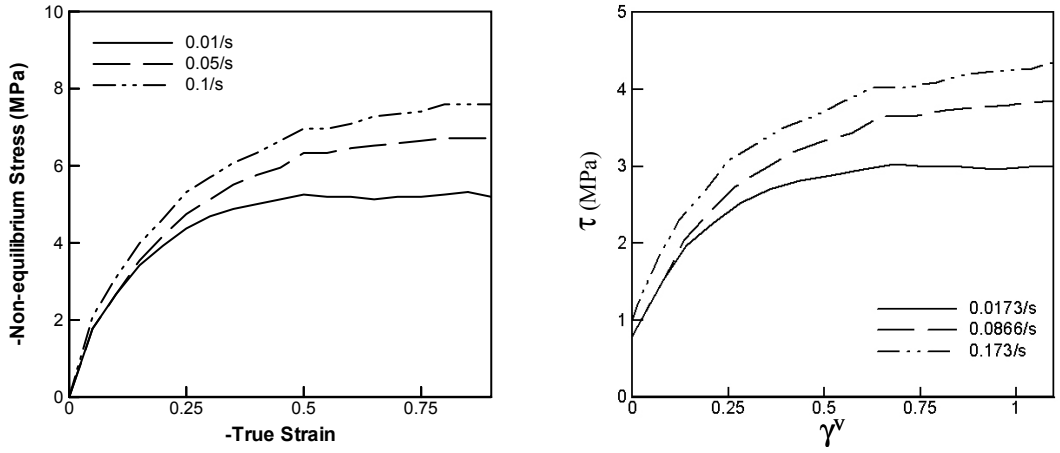

(a) (b)

Figure A4: (a) T^V vs ε plots at different strain rates; (b) τ - γ^v plots at different strain rates.

From Figure A4(b), the equivalent shear stress at each equivalent shear strain rate approximates to a constant value at large equivalent shear strain. For $\dot{\gamma}_1^v = 0.0173/s$ (from $\dot{\varepsilon} = 0.01/s$), $\tau_1 = 2.9MPa$; for $\dot{\gamma}_2^v = 0.0866/s$ (from $\dot{\varepsilon} = 0.05/s$), $\tau_2 = 3.8MPa$; for $\dot{\gamma}_3^v = 0.173/s$ (from $\dot{\varepsilon} = 0.1/s$), $\tau_3 = 4.3MPa$. Using least square fit gives $c = 0.60$, $b = 5.3$.

From eqn (A7), we obtained

$$\dot{\gamma}_0 = e^{D-8.3}, \qquad \text{(A8a)}$$

$$D = \frac{s_0}{0.60}. \qquad \text{(A8b)}$$

Using a kinked model, Argon (1973) and Argon and Bessonov (1977) predicted for a wide range of glassy polymers,

$$s = \frac{0.077G}{1-v}. \qquad \text{(A9)}$$

Although the resistance to flow is a more complicated mechanism in the TPU, we use this expression as a guideline. From eqn(A9), $s \sim 2.52MPa$. $s_0 = 2.52MPa$ was thus used as a starting point for identifying material parameters. From eqn. (A8), we obtained $\dot{\gamma}_0 = 1.94\times10^{-2}$ and $\Delta G = 1.81\times10^{-20} J$.

References

Argon, A.S., 1973. A theory for the low temperature plastic deformation of glassy polymers. Phil. Mag., 28, 839-865.

Argon, A.S., Bessonov, M.I., 1977. Plastic deformation in polyimides, with new implications on the theory of plastic deformation of glassy polymers. Phil. Mag., 35, 917-933.

Arruda, E.M., Boyce, M.C., 1993. A Three-dimensional constitutive model for the large stretch behavior of elastomers. J. Mech. Phys. Solids, 41, 389-412.

Beatty, M.F., Krishnaswamy, S., 2000. A theory of stress-softening in incompressible isotropic materials. J. Mech. Phys. Solids, 48, 1931-1965.

Bergstrom, J., Boyce, M.C., 1999. Mechanical behavior of particle filled elastomers. Rubber Chem. Tech., 72, 633-656.

Bergstrom, J.S., Boyce, M.C., 2000. Large strain time-dependent behavior of filled elastomers. Mech. Mater., 32, 627-644.

Blanchard, A.F., Parkinson, D., 1952. Breakage of carbon-rubber networks by applied stress. Ind. Eng. Chem., 44, 799.

Bonart, R., 1968. X-ray investigations concerning the physical structure of cross-linking in urethane elastomers. J. Macromol. Sci., Phys, B2, 115.

Bonart, R., Morbitzer, L., Hentze, G., 1969. X-ray investigations concerning the physical structure of cross-linking in urethane elastomers, II. J. Macromol. Sci. Phys., B3, 337-356.

Bonart, R., Muller-Riederer, G., 1981. Modellvorstellungen zur molekulorientierung in gedehnten segmentierten polyurethan elastomeren. Colloid Polym. Sci., 259, 926-936.

Boyce, M.C., Socrate, S., Yeh, O.C., Kear, K., Shaw, K., 2001a. Micromechanisms of Deformation and Recovery in Thermoplastic Vulcanizates. J. Mech. Phys. Solids, 49, 1073-1098.

Boyce, M.C., Yeh, O.C., Socrate, S., Kear, K., Shaw, K., 2001b. Micromechanisms of the Cyclic Softening in Thermoplastic Vulcanizates. J. Mech. Phys. Solids, 49, 1343-1360.

Boyce, M.C., Kear, K., Socrate, S., Shaw, K., 2001c. Deformation of thermoplastic vulcanizates. J. Mech. Phys. Solids, 49, 1073-1098.

Boyce, M.C., Parks, D.M., Argon, A.S., 1988. Large inelastic deformation of glassy polymers, Part I: rate dependent constitutive model. Mech. Mater., 7, 15-33.

Bueche, F., 1960. Molecular basis for the Mullins effect. J. Appl. Polym. Sci., 4, 107-

114.

Bueche, F., 1961. Mullins effect and rubber-filler interaction. J. Appl. Polym. Sci. 5, 271-281.

Chen-Tsai, C.H.Y., Thomas, E.L., MacKnight, W.J., Schneider, N.S., 1986. Structure and morphology of segmented polyurethanes. 3. Electron microscopy and small angle X-ray scattering studies of amorphous random segmented polyurethanes. Polym., 27, 659.

Cooper, S.L., Tobolsky, A.V., 1966. Properties of linear elastomeric polyurethanes. J. Polym. Sci., 10, 1837-1844.

Cooper, S.L., Huh, D.S., Morris, W.J., 1976. Encyclopedia of Polymer Science and Technolgy, Supplementary Volume, Wiley, New York, 521.

Dannenberg, E.M., 1974. The effects of surface chemical interactions on the properties of filler-reinforced rubbers. Rubber Chem. Tech., 48, 410-444.

Dorfmann, A., Ogden, R.W., 2003. A pseudo-elastic model for loading, partial unloading and reloading of particle-reinforced rubber. Int. J. Solids Struct., 40, 2699-2714.

Estes, G.M., Seymour, R.W., Cooper, S.L., 1971. Infrared studies of segmented polyurethane elastomers. II, Macromol., 4, 452-457.

Govindjee, S., Simo, J., 1991. A micro-mechanically based continuum damage model for carbon black-filled rubbers incorporating Mullin's effect. J. Mech. Phys. Solids, 39, 87-112.

Govindjee, S., Simo, J., 1992. Transition from micro-mechanics to computationally efficient phenomenology: carbon black filled rubbers incorporating Mullins' effect. J. Mech. Phys. Solids, 40, 213-233.

Harwood, J.A.C., Mullins, L., Payne, A.R., 1965. Stress softening in natural rubber vulcanizates, Part II. J. Appl. Polymer Sci., 9, 3011-3021.

Harwood, J.A.C., Payne, A.R., 1966a. Stress softening in natural rubber vulcanizates, Part III. J. Appl. Polymer Sci., 10, 315-324.

Harwood, J.A.C., Payne, A.R., 1966b. Stress softening in natural rubber vulcanizates, Part IV. J. Appl. Polymer Sci., 10, 1203-1211.

Hepburn, C., 1982. Polyurethane Elastomers, Applied Science, London.

Horgan, C.O., Ogden, R.W., Saccomandi, G., 2003. A theory of stress softening of elastomers based on finite chain extensility. To be appeared in Proc. R. Soc. Lond. A.

Johnson, M.A., Beatty, M.F., 1993a. The mullins effect in uniaxial extension and its influence on the transverse vibration of a rubber string. Comtinuum Mech. Thermodyn., 5, 83-115.

Johnson, M.A., Beatty, M.F., 1993b. A constitutive equation for the Mullins effect in stress controlled uniaxial extension experiments. Comtinuum Mech. Thermodyn., 5, 301-318.

Kimura, I., Ishihara, H., Ono, H., Yashihara, N., Nomura, S., Kawai, H., 1974. Morphology and deformation mechanism of segmented poly(urethaneureas) in relation to spherulitic crystalline textures. Macromol., 7, 355-363.

Koutsky, J.A., Hien, N.V., Cooper, S.L., 1970. Some results on electron microscope investigations of polyether-urethane and polyester-urethane block copolymers. Polymer Lett., 8, 353-359.

Lion, A., 1996. A constitutive model for carbon black filled rubber, experimental investigation and mathematical representation. Continuum Mech. Thermodyn., 6,

153-169.

Lion, A., 1997. A physically based method to represent the thermo-mechanical behavior of elastomers. Acta Mechanica, 123, 1-25.

Marckmann, G.,Verron, E., Gornet, L., Chagnon, G., Charrier, P., Fort, P., 2002. A theory of network alteration for the Mullins effect. J. Mech. Phys. Solids, 50, 2011-2028.

Medalia, A.I., Kraus, G., 1994. Science and Technology of Rubber, Academic Press Inc., New York.

Miehe, C., Keck, J., 2000. Superimposed finite elastic-viscoelastic-plastoelastic response with damage in filled rubbery polymers: Experiments, modeling and algorithmic implementation. J. Mech. Phys. Solids, 48, 323-365.

Mullins, L., Tobin, N.R., 1957. Theoretical model for the elastic behavior of filler-reinforced vulcanized rubber. Rubber Chem. Technol., 30, 555-571.

Mullins, L., Tobin, N.R., 1965. Stress softenings in natural rubber vulcanizates, Part I. J. Appl. Polymer Sci., 9, 2993-3010.

Mullins, L., 1969. Softening of rubber by deformation. Rubber Chem. Tech., 42, 339-362.

Ogden, R.W, Roxburgh, D.G., 1999a. A pseudo-elastic model for the Mullins effect in filled rubber, Proc. R. Soc. Lond. A, 455, 2861-2877.

Ogden, R.W, Roxburgh, D.G., 1999b. An energy-based model of the Mullins effect, in Proceedings of the First European Conference on Constitutive Models for Rubber, Belkema, Rotterdam.

Payne, M.T., Rader, C.P., 1993. Thermoplastic elastomers: a rising start, in: Elastomer

Technology Handbook (ed. By Cheremisinoff, N.P.), CRC press.

Petrovic, Z., Ferguson, J., 1991. Polyurethane Elastomers. Prog. Polym. Sci., 16, 695-836.

Qi, J.H., Boyce, M.C., 2004. Constitutive Model for Stretch-Induced Softening of the Stress-Stretch Behavior of Elastomeric Materials. J. Mech. Phys. Solids., available online as Article in Press.

Rigbi, Z., 1980. Reinforcement of rubber by carbon black. Adv. Poly. Sci., 36, 21-68.

Sauer, B.B., Mclean, R.S., Brill, D.J., Londono, D.J., 2002. Morphology and orientation during the deformation of segmented elastomers studied with small-angle X-ray scattering and atomic force microscopy. J. Ploym. Sci., 40, 1727-1740.

Sequela R., Prudhomme, J., 1978. Effects of casting solvents on mechanical and structural properties of polydiene-hydrogenated polystyrene-polyisoprene-polystyrene and polystyrene-polybutadiene-polystyrene block copolymers. Macromol., 11, 1007-1016.

Schollenbenger, C.S., Scott, H., Moore, G.R., 1958. Polyurethane VC, a virtually crosslinked elastomer. Rubber World, 137, 549.

Simo, J.C., 1987. On a fully three-dimensional finite-strain viscoelastic damage model: formulation and computational aspects. Compu. Method Appl. Mech. Eng., 60, 153-173.

Smith, T.L., 1974. Tensile strength of polyurethane and other elastomeric block copolymers. J. Ploym. Sci., 12, 1825-1848.

Sung, C.S.P., Smith, T.W., Hu, C.B., Sung, N.H., 1979. Hysteresis behavior in polyether poly(urethaneureas) based on 2,4-toluene diisocyanate, ethylenediamine, and

poly(tetramethylene oxide). Macromol., 12, 538-540.

Sung, C.S.P., Hu, C.B., Wu, C.S., 1980a. Properties of segmented poly(urethaneureas) based on 2,4-toluene diisocyanate I. Macromol., 13, 111-116.

Sung, C.S.P., Smith, T.W., Sung, N.H., 1980b. Properties of segmented poly(urethaneureas) based on 2,4-toluene diisocyanate, II. Macromol., 13, 117-121.

Wang, C.B., Cooper, S.L., 1983. Morphology and properties of segmented polyether polyurethaneureas. Macromol. 16, 775-786.

Wilkes, G.L., Abouzahr, S., 1981. SAXS studies of segmented polyesther poly(urethaneurea) elastomers. Macromol., 14, 456-458.

Yeh, F., Hsiao, B.S., Sauer, B.B., Michel, S., Siesler, H.W., 2003. In situ studies of structure development during deformation of a segment poly(urethane-urea) elastomer. Macromol., 36, 1940-1954.